Virus Genes (2016) 52:759–767
DOI 10.1007/s11262-016-1366-2

Influenza A Virus-induced expression of ISG20 inhibits viral replication by interacting with nucleoprotein

Hongren Qu[1] · Jing Li[2] · Limin Yang[2] · Lei Sun[2] · Wenjun Liu[2] · Hongxuan He[1]

Received: 3 March 2016 / Accepted: 18 June 2016 / Published online: 24 June 2016

Abstract Influenza A virus (IAV) is an important pathogen that has a wide range of hosts and represents a threat to the health of humans and several animal species. IAV infection can induce the transcription of many genes in the host. In the present study, we demonstrated for the first time that three different strains of H1N1 IAV induce the expression of an IFN-stimulated gene, ISG20. We determined the antiviral activity of ISG20 against IAV because ISG20 inhibited viral protein expression and reduced the progeny viral titer dependent upon its exonuclease activity. To elucidate the detailed mechanism of ISG20, we further demonstrated that ISG20 impairs the polymerase activity and inhibits both the replication and transcription levels of the M1 and NP genes. Notably, we identified that ISG20 colocalizes and interacts with NP during IAV infection, while exonuclease-inactive mutant ISG20 lacked association with NP, indicating that ISG20 inhibits IAV replication by interacting with NP. Together, these data provide a detailed explanation for the specific antiviral action of ISG20 and suggest that ISG20 may act as a promising antiviral drug candidate against IAV.

Edited by Zhen F. Fu.

✉ Wenjun Liu
liuwj@im.ac.cn

✉ Hongxuan He
hehx@ioz.ac.cn

[1] National Research Center for Wildlife-Borne Diseases, Institute of Zoology, Chinese Academy of Sciences, 100101 Beijing, China

[2] CAS Key Laboratory of Pathogenic Microbiology and Immunology, Institute of Microbiology, Chinese Academy of Sciences, 100101 Beijing, China

Keywords IFN-stimulated gene · Polymerase activity · Exonuclease

Introduction

Influenza A virus (IAV) belongs to the *Orthomyxoviridae* family. Its genome consists of eight segments of negative-sense single-stranded RNA that encode up to 14 viral proteins, including the polymerase proteins (PB1, PB2, and PA), nucleoprotein (NP), the membrane proteins hemagglutinin (HA) and neuraminidase (NA), matrix proteins (M1 and M2), the nonstructural protein (NS1), nuclear export protein (NEP), and four newly identified proteins (PB1-F2, PB1 N40, PA-X, and M42) [1–5]. According to the serological characteristics of the two membrane proteins HA and NA, IAVs are categorized into different subtypes: 18 types of HA and 11 types of NA [6, 7].

Some subtypes of IAV can cause acute respiratory diseases and seasonal pandemics (and even annual epidemics) in hosts, such as the Spanish influenza in 1918, the Asian influenza in 1957, the Hong Kong influenza in 1968, and the recently reported swine-origin H1N1 2009 pandemic influenza in 2009 [8]. Thus, there is an urgent need for effective antiviral drugs. At the cellular level, IAV infection induces dramatic changes in host transcription. To date, high-throughput RNA sequencing (RNA-seq) has been the most valuable method developed to systemically explore transcriptomics. Thousands of genes that undergo transcriptional regulation after IAV infection have been identified via RNA-seq by several groups [9–12]. Gene ontology enrichment and pathway analysis demonstrate that the regulated genes are involved in various biological processes, including immune responses, cell adhesion, cell metabolism, antigen presentation, and signal transduction.

Notably, among these biological processes, most genes focus on immune response regulation [9, 13].

The ISG20 gene was identified on the basis of induced expression level by both type I and type II IFNs in several cell lines and encodes an IFN-stimulated gene product of 20 kDa [14]. Biochemical assays and sequence alignments demonstrate that ISG20 belongs to the 3′–5′ exonuclease super family, but it displays higher affinity for RNA substrates than for DNA [15]. The crystal structure of ISG20 demonstrates that the characteristic structure of ISG20's active center is highly similar to other DNases. Nevertheless, the recognition mechanism of ISG20 for glycosylated nucleotides is slightly different from that of DNase. The active sites of ISG20 harbor the preference for RNA substrates. The crystal structural preference for UMP is also in accordance with the higher affinity for RNA in biochemical assays [16].

Besides IFN, ISG20 is also induced by infection of several viruses. ISG20 is induced in hepatitis B virus (HBV) transgenic mouse hepatocyte cell lines during IFN-mediated suppression of viral replication [17] and in the liver of acutely HBV-infected chimpanzees during virus clearance [18]. Moreover, expression of the ISG20 gene is induced by infection of Rabies virus (RABV) in neuron-derivative cell lines [19], Epstein-Barr virus (EBV) in B lymphocytes [20], and cytomegalovirus in fibroblasts [21]. In addition, expression of the Vpr protein of human immunodeficiency virus type 1 (HIV-1) in monocyte-derived dendritic cells (MDDCs) up-regulates expression of ISG20 [22].

The up-regulation of ISG20 during infection by several viruses indicates that ISG20 may play an important role in antiviral responses. In accordance with the preference for RNA substrates in biochemical assays, ISG20 displays antiviral activity against several single-stranded RNA viruses, including yellow fever virus, vesicular stomatitis virus (VSV), encephalomyocarditis virus (EMCV), and hepatitis C virus (HCV) [23–25]. In addition, ISG20 also shows resistance against both the double-stranded RNA virus HIV-1 and the DNA virus HBV [26, 27], and the antiviral activity of ISG20 is dependent on its exonuclease activity.

As mentioned above, ISG20 displays antiviral activity against several viruses, and the present study aimed to elucidate whether ISG20 exerts antiviral effects on IAV and understand its specific molecular mechanisms. First, ISG20 was expressed in 293T cells, and the effects of ISG20 on IAV protein expression and gene replication and transcription were assayed by western blotting and real-time PCR. The viral protein that interacted with ISG20 was also further identified.

Materials and methods

Cell lines, viruses, and antibodies

Human embryonic kidney 293T cells (293T cells), human alveolar epithelial A549 cells (A549 cells), and Madin-Darby Canine Kidney MDCK cells (MDCK cells) lines were maintained in Dulbecco's modified Eagle's medium (GIBCO) supplemented with 10 % heat-inactivated fetal bovine serum (GIBCO). Influenza A virus strains A/WSN/33 (WSN), A/Puerto Rico/8/1934 (PR8), and A/California/04/2009 (CA04) were propagated in the allantoic cavities of 10-day-old specific pathogen-free (SPF) embryonic chicken eggs at 37 °C for 2 days.

Mouse anti-M1 monoclonal antibody, rabbit anti-NP polyclonal antibody, and rabbit anti-ISG20 polyclonal antibody were prepared as previously described [28, 29]. Mouse anti-β-actin monoclonal antibody and anti-Myc monoclonal antibody were purchased from Santa Cruz Biotechnology. FITC-conjugated anti-rabbit IgG and TRITC-conjugated anti-mouse IgG were purchased from ZhongyuanBaihui Biotechnology (Beijing, China).

Plasmid construction

For mammalian cell expression, the coding sequence of ISG20 was cloned into pCMV-Myc and pcDNA3.0. ISG20-D94G, in which the aspartic acid at position 94 of ISG20 was replaced with glycine, was constructed with a Newpep site-directed mutagenesis kit (China) following the manufacturer's instructions. The positive control plasmid pCMV-Myc-IFIT2 was constructed as previously described [30]. For luciferase assays, the expression plasmids for the PA, PB1, and PB2 genes from the A/WSN/33 virus were generated by cloning into the pCDNA3-FLAG vector as previously described [29].

Cell transfection and virus infection

293T cells were seeded in 6-well plates and incubated for 16–20 h. When the confluence exceeded 90 %, the cells were transfected with empty vector or plasmids containing ISG20 by Lipofectamine^{TM} 2000 (Invitrogen) following the manufacturer's instructions. At 24 h post-transfection, cells were infected with WSN at a MOI of 0.01. At 16 h post-infection (p.i.), the cells were lysed with lysis buffer for western blotting. The medium for infection was FBS-free and contained 0.5 μg/ml TPCK-treated trypsin. The MOI was 0.01 for western blotting and real-time PCR, and 1.0 for immunofluorescence.

RNA extraction and quantification by real-time PCR

293T cells and A549 cells were transfected with ISG20 plasmids or empty plasmid and then infected with WSN at a MOI of 0.01. Cell samples were collected at 0, 4, 8, and 12 h p.i. (hours post-infection) for RNA isolation as previously described [31]. The RNA samples were treated with DNase I (TaKaRa) at 37 °C for 30 min. Total RNA was reverse transcribed into cDNAs of mRNA, vRNA, or cRNA using 10 pmol of oligo-dT primer, vRNA-specific primer, or cRNA-specific primer. The exonuclease activity of AMV reverse transcriptase was then heat inactivated at 95 °C for 5 min.

Primer sequences and real-time PCR programs are described in previous studies [29]. Dissociation curve analysis was performed after each assay to ensure specific target detection. The resulting mRNA levels were normalized to the housekeeping gene GAPDH. All data and standard deviations were determined from three independent experiments.

RNA preparation and Solexa/Illumina sequencing (RNA-seq)

293T cells and A549 cells were infected with WSN, PR8, or CA04 at MOI = 2, and cells were harvested for RNA isolation at 8 h p.i.. All of the RNA Integrity Number (RIN) values were >7.0, and the 28S:18S rRNA ratios were >1.9, as confirmed using an Agilent Bioanalyzer. Total cellular RNA was analyzed by RNA-seq as previously described [32].

Luciferase reporter assays for influenza polymerase complex activity

The luciferase reporter assays were performed as previously described [33] with slight modification. In brief, all polymerase complex component plasmids (0.1 μg each) were cotransfected with a luciferase reporter plasmid (0.25 μg) that contained noncoding sequence from the NS segment of the IAV genome and the luciferase gene that was driven by the PolI promoter into 293T cells. At the same time, pCMV-Myc empty vector or plasmid expressing ISG20(s) (wild-type or mutant ISG20, 0.25 μg) was also transfected into 293T cells. At 36 h post-transfection, cell lysates were prepared using a luciferase assay kit (Promega), and the relative activities were compared to the control group. A plasmid expressing β-galactosidase (0.1 μg) was cotransfected as an internal control for data normalization.

Plaque assay

Plaque assay was performed as previously described [33]. In brief, MDCK cell monolayers (5×10^6 cells at 100 % confluence in 12-well plates) were washed with phosphate-buffered saline (PBS) and infected with different dilutions of virus for 1 h at 37 °C. The virus inoculums were removed by washing with PBS. Cell monolayers were then overlaid with agar overlay medium (DMEM supplemented with 1 % low melting point agarose and 1 μg/ml TPCK-treated trypsin) and incubated at 37 °C. Visible plaques were counted at 3 days post-infection, and the virus titers were determined. All data are expressed as means for three independent experiments.

Indirect immunofluorescence assays

The indirect immunofluorescence assays were performed as previously described [33]. In brief, the 293T cells, growing on glass cover slips, were infected with WSN at a MOI of 1. The cells were then washed with PBS three times, fixed in 4 % paraformaldehyde for 30 min at room temperature, and blocked with 4 % BSA in PBST (0.5 % Triton X-100 in PBS) for 1 h at 37 °C or overnight at 4 °C. The cells were then stained with rabbit anti-NP polyclonal antibody and mouse anti-Myc monoclonal antibody. After washing with PBST five times (10 min/wash), the cells were then stained with FITC-conjugated anti-rabbit IgG and TRITC-conjugated anti-mouse IgG. All of the antibodies were diluted in 4 % BSA. Cell nuclei were stained with 5 mg/ml DAPI (Sigma) in PBS. Following staining, cover slips were analyzed using an LSCMFV500 confocal microscope.

Coimmunoprecipitation assay (co-IP)

293T cells were transfected with FLAG-tagged ISG20(s) and then infected with A/WSN/33 (MOI = 0.1). At 12 h p.i., the cells were lysed in binding buffer supplemented with protease inhibitor cocktail. The cell lysates were immunoblotted with anti-FLAG antibody to confirm the expression of the genes of interest in the 293T cells, and then, the co-IP assays were performed using anti-FLAG M2 affinity gel. The immunoprecipitated proteins were assayed with an anti-NP polyclonal antibody.

Results

Infection of IAV up-regulated the expression of ISG20

293T cells and A549 cells were infected with three different strains of H1N1 subtype IAV (WSN, PR8, and CA04). At 8 h p.i,, the cellular RNA was isolated for RNA-seq. As shown in Fig. 1a, the three IAV strains induced the mRNA expression of ISG20 by 3- to 5-fold. To further validate the results obtained from RNA-seq, the up-regulation of ISG20 by IAV was further confirmed using real-

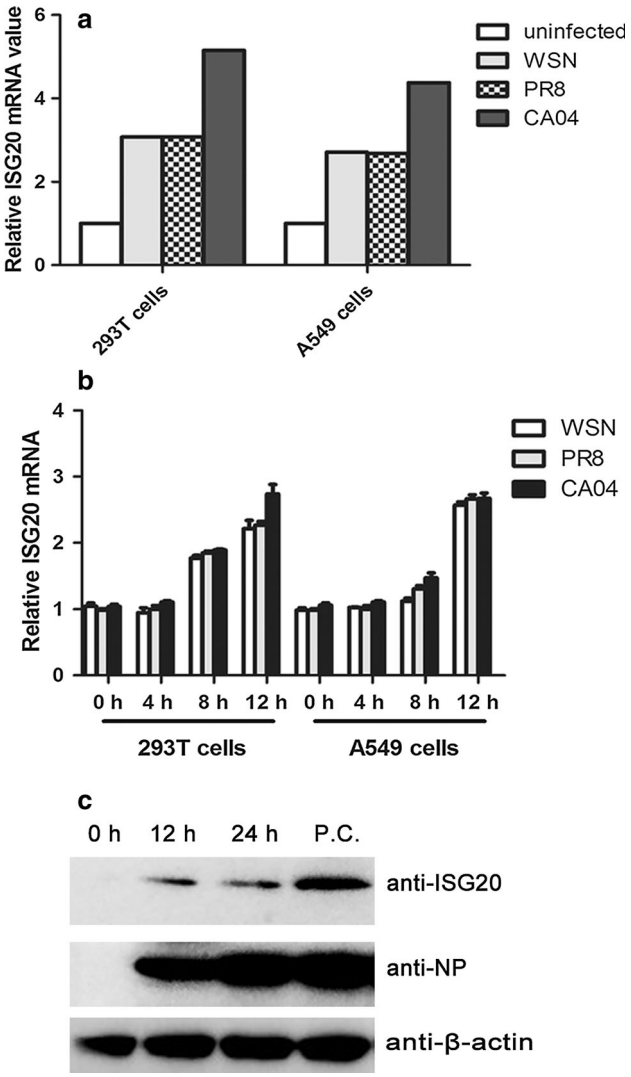

Fig. 1 The mRNA and protein expression of ISG20 induced by IAV was identified by RNA-seq (**a**), real-time PCR (**b**), and western blotting (**c**). **a** 293T cells and A549 cells were infected with WSN, PR8, or CA04 (MOI = 2). At 8 h p.i., cells were harvested for RNA isolation, and total cellular RNA was analyzed by RNA-seq. The relative mRNA value of ISG20 is shown. **b** 293T cells and A549 cells were infected with WSN, PR8, or CA04 (MOI = 0.01). Cells were harvested for RNA isolation at the indicated time points. The relative quantification of ISG20 mRNA was assayed by real-time PCR. The specificities of the amplified products were confirmed by melting curve analysis. In all of the PCR assays, GAPDH was used as an internal control. Data are mean ± SD of three independent experiments. **c** A549 cells were infected with WSN (MOI = 0.01). At the indicated time points, cells were harvested and lysed for western blotting. P.C.: the positive control. A549 cells were transfected with pCMV-Myc-ISG20. At 16 h post-transfection, cells were infected with WSN for 24 h

time PCR. Similar up-regulation of ISG20 by the three IAV strains is shown in Fig. 1b. Furthermore, the protein expression of ISG20 was detected in WSN-infected A549 cells at 12 h p.i. (Fig. 1c). These data proved that infection of IAV induced the expression of ISG20.

ISG20 inhibited the protein expression and polymerase activity of IAV

To identify the antiviral activity of ISG20 against IAV, we first tested the effect of ISG20 on IAV protein expression. ISG20 and ISG20-D94G, which lacks exonuclease activity [15], were cloned into vector pCMV-Myc and expressed in 293T cells. After transfection with the indicated plasmid, 293T cells were then infected with IAV. The cells were subsequently lysed for western blotting to detect the M1 and NP protein. As shown in Fig. 2a, ISG20 significantly inhibited the M1 and NP protein levels, and the inhibition of M1 was more potent than that of NP. However, ISG20-D94G restored the M1 and NP protein levels comparable to the empty vector control. These results indicated that ISG20 inhibits IAV protein expression through its exonuclease. To confirm the suppressive function of ISG20 on IAV replication, we further determined if ISG20 affects the progeny viral titer of IAV by plaque assays. The reported anti-influenza virus ISG-IFIT2, which inhibited viral replication and reduced the progeny viral titer and the polymerase activity of IAV [30, 34], was chosen as the positive control. The expression of Myc-tagged ISG20(s) and IFIT2 was identified by western blotting (Fig. 2d). In accordance with the above results, ISG20 reduced the progeny viral titer by roughly 67 % compared to the control group, but ISG20-D94G did not (Fig. 2b). The inhibition effect of ISG20 was comparable with that of IFIT2.

We further investigated whether ISG20 regulates IAV polymerase activity because the transcription of IAV is accomplished by its polymerase complex. 293T cells were cotransfected with plasmids-encoding polymerase complex components, together with ISG20(s) plasmid or the positive control plasmid pCMV-Myc-IFIT2. At 36 h post-transfection, cell lysates were harvested for luciferase assays. We found that ISG20 decreases polymerase activity by 30 % (Fig. 2c), while ISG20-D94G antagonized the suppressive effect of wild-type ISG20 on polymerase activity and improved the activity by 20 % compared to the control, which was coincident with the enhanced M1 and NP protein levels in Fig. 2a. These results indicate that ISG20 enacts its antiviral activity against IAV by reducing viral polymerase activity.

ISG20 inhibited viral replication and transcription

To identify the exact stage of the IAV life cycle regulated by ISG20, real-time PCR was performed to detect the replication and transcription levels of IAV. As shown in Fig. 3, ISG20 inhibited all of the mRNA, vRNA, and cRNA levels of the M1 and NP genes, but the inhibitory effect on the mRNA levels was more significant than that on the vRNA and cRNA levels. Moreover, the inhibition on the mRNA level of M1 was more potent than that of NP, which is in accordance with the more potent inhibition of the protein level of M1 in Fig. 1a. These results suggest

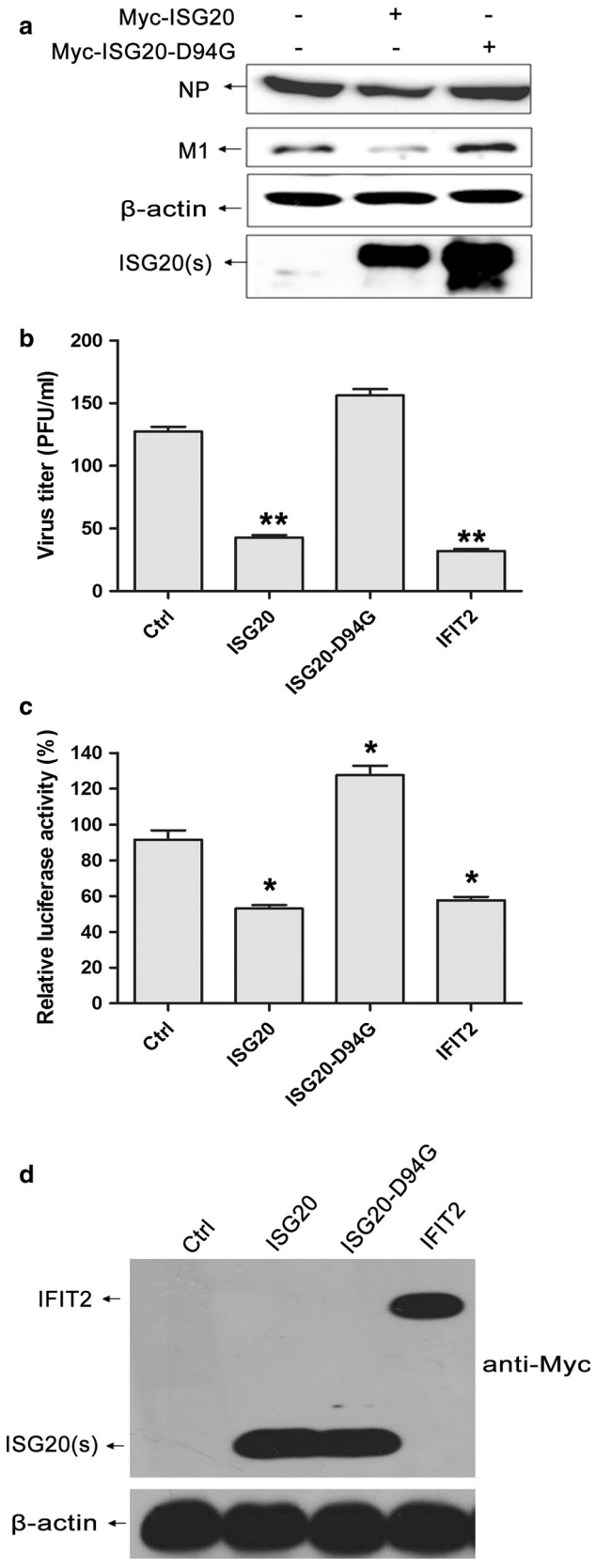

◀**Fig. 2** ISG20 inhibited the replication of IAV through its exonuclease activity. **a** Wild-type (ISG20) or exonuclease activity-defective mutant ISG20-D94G (the pCMV-Myc empty plasmid was used as control) was transfected into 293T cells, which were then infected with WSN (MOI = 0.01). At 16 h p.i., cell lysates were analyzed by western blotting with a monoclonal anti-Myc antibody, monoclonal anti-M1 antibody, and polyclonal anti-NP antibody; β-actin was used as a control. ISG20(s): ISG20 or ISG20-D94G. **b** The effect of wild-type and mutant ISG20 on the viral titer of IAV was assayed by standard phage assays. 293T cells were transfected with ISG20(s) or the positive control IFIT2 and then infected with WSN (MOI = 1). At 12 h p.i., infectious progeny viral particles generated from infected cells were quantified by standard plaque assays. Data are shown as mean ± SD ($n = 3$). **c** The effect of wild-type and mutant ISG20 on the polymerase activity of IAV was assayed by luciferase assays. Data are shown as the mean ± SD ($n = 3$). The Mann–Whitney U test was used to compare the differences between the experimental groups and the control group. A value of $P < 0.05$ was considered statistically significant. $^{*}P < 0.05$ and $^{**}P < 0.01$. **d** The expression of Myc-tagged ISG(s) or IFIT2 was identified by monoclonal antibody against Myc-tag

that ISG20 both inhibits viral protein expression and reduces viral replication and transcription, which is an important conceptual advance over the previous study [23].

ISG20 colocalized and interacted with NP

Because ISG20 inhibited the polymerase activity of IAV, and NP is one of the components of the viral ribonucleoprotein (vRNP) complex, we wondered whether ISG20 interacts with the NP protein. We first determined the cellular location of NP by indirect immunofluorescence. As shown in Fig. 4a, ISG20 colocalized with NP in the cytoplasm. The interaction between ISG20 and NP was further confirmed by co-IP (Fig. 4b), and the exonuclease-defective mutant ISG20-D94G did not display this association with the virus. Moreover, both wild-type and mutant ISG20 mainly localized in the cytoplasm. At 12 h p.i., NP was mainly localized in the cytoplasm in cells transfected with any of the three plasmids (empty vector, ISG20, or ISG20-D94G), suggesting that ISG20 did not influence the cellular location of NP. These results further validated that ISG20 restricts the infection of IAV by interacting with NP, while whether ISG20 interacted with NP directly remains to be further elucidated because ISG20 may sequester the RNA molecule(s) bound to NP due to its high affinity for RNA substrates [15], and thus interacted with NP indirectly.

Discussion

RNA-seq demonstrated that infection by three different strains of H1N1 IAV (WSN, PR8, and CA04) up-regulated the expression of many genes in 293T cells, and the growth curves of the three viruses did not display significant differences (data not shown). Because interferon (IFN) plays

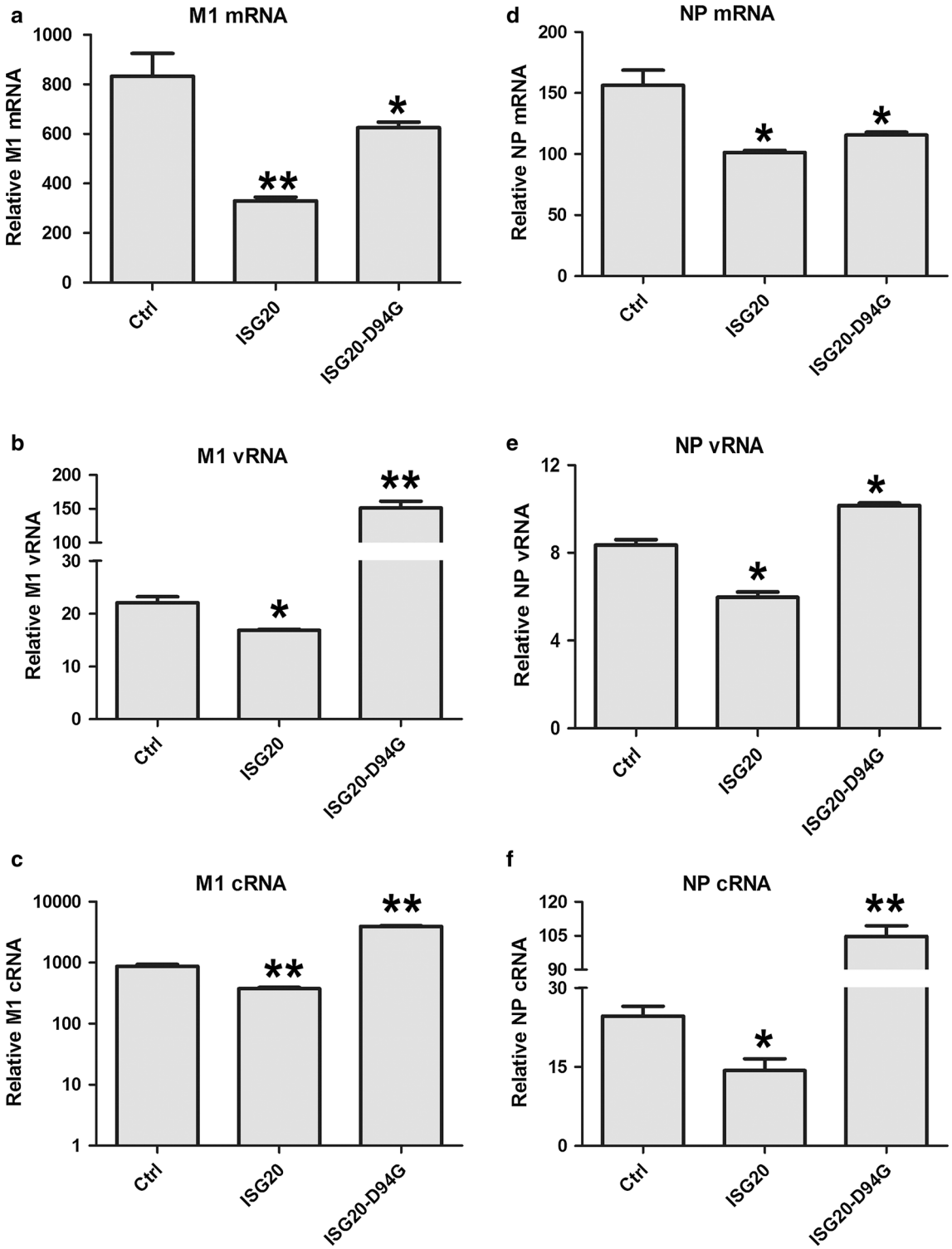

Fig. 3 ISG20 impaired both the replication and the transcription levels of IAV. ISG20(s) was transfected into 293T cells, which were then infected with WSN (MOI = 0.1). At 8 h p.i., cells were harvested for total RNA extraction. Different primers were used for cDNA synthesis of mRNA, vRNA, and cRNA to relatively quantify the M1 and NP genes by real-time PCR. The specificity of the amplified products was confirmed by melting curve analysis. GAPDH was used as an internal control. Data are shown as the mean ± SD ($n = 3$). The Mann–Whitney U test was used to compare the differences between the experimental groups and the control group. A value of $P < 0.05$ was considered statistically significant. $^{*}P < 0.05$ and $^{**}P < 0.01$

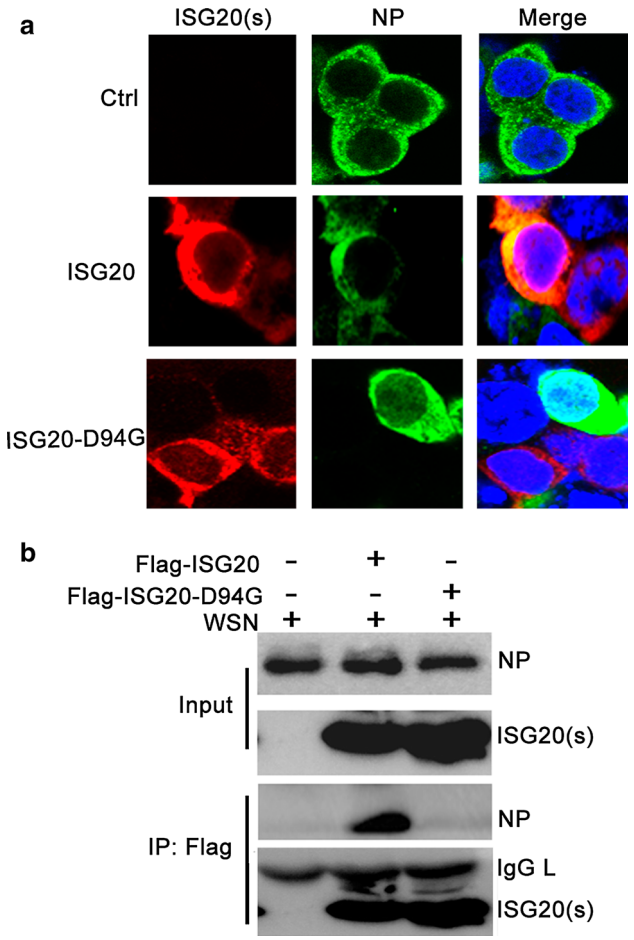

Fig. 4 ISG20 colocalized and interacted with NP of IAV during infection. **a** The localization of the IAV NP protein was assayed in 293T cells transfected with wild-type or ISG20-D94G plasmid by immunofluorescence. At 12 h p.i., cells were fixed, blocked, and stained with anti-Myc (*red*), anti-NP (*green*), and DAPI (*blue*). **b** The interaction of ISG20 with NP during virus infection was determined by co-IP. 293T cells were transfected with FLAG-tagged ISG20(s), and then infected with WSN (MOI = 0.1). At 12 h p.i., cell lysates were incubated with anti-FLAG M2 affinity beads for co-IP. IgG L: IgG light chain (Color figure online)

important roles in anti-IAV responses, IFN-stimulated genes (ISGs) are of interest to us. Thirty-two ISGs were up-regulated by all three viruses. Among these ISGs, some are known to possess antiviral activities against several viruses. In the present study, ISG20 was selected for functional investigations because several lines of evidence show that ISG20 inhibits RNA virus replication, but the detailed mechanism remains unknown [25, 26]. The present study demonstrated, for the first time, that ISG20 inhibits viral genome replication, transcription, and protein expression of IAV, impairs IAV polymerase activity, and interacts with NP, which is an important conceptual advance over the previous study and provides a more exact explanation for the antiviral mechanism of this IFN-inducible protein.

The only reported evidence of ISG20's antiviral activity against IAV is that stable-expression of ISG20 in HeLa cells reduces the virus yield [23]. However, the specific mechanism of inhibition was elusive. We wondered which step of the viral life cycle is targeted by ISG20 and whether ISG20 interacts with any viral proteins. With these questions in mind, we first detected the inhibitory effect of ISG20 on IAV protein levels. As shown in Fig. 2a, ISG20 inhibited the expression of M1 and NP protein. ISG20 displayed direct inhibition on IAV because ISG20 reduced the progeny viral titer in 293T cells (Fig. 2b), which is consistent with the reported results in HeLa cells [23].

Furthermore, we determined for the first time that ISG20 exerts its suppressive impact on the polymerase activity of IAV (Fig. 2c). Because the replication and transcription of IAV are completed by the polymerase complex, we speculated that ISG20 inhibits the transcription and replication of IAV because expression of ISG20 reduced mRNA and vRNA levels (Fig. 3). We found that ISG20 exerts its antiviral activity against IAV by reducing viral polymerase activity. The polymerase complex is a critical component of the viral structure, and inhibition of the polymerase activity reflected the extensive effect of ISG20 on the viral life cycle. Several proteins and compounds inhibit IAV replication by reducing viral polymerase activity [35–37]. For instance, the multiple kinase inhibitor WV970 inhibits RNA expression and polymerase activity of IAV and was identified as a novel antiviral drug candidate [36]. There are several mechanisms on how ISG20 inhibit the polymerase activity. ISG20 may interact with component(s) of the polymerase complex, which is confirmed in Fig. 4 that ISG20 interacted with NP. Another possibility is that overexpression of ISG20 may result in viral RNA degradation, which is confirmed in Fig. 3 that ISG20 decreased the viral RNA level. Meanwhile conversely, the inhibition of polymerase activity would result in the viral RNA degradation, while the exact mechanism that ISG20 adopted to inhibit the polymerase activity of IAV remains elusive.

In accordance with previous reports, the inhibitory effect of ISG20 on IAV was dependent on its exonuclease activity, and the ISG20-D94G mutant even boosted the IAV protein levels, polymerase activity, and viral titer to some extent. This was mainly due to the dominant-negative effect of ISG20-D94G, and the same dominant-negative effect of ISG20-D94G was reported for HCV RNA replication [23, 25]. A previous report also demonstrates that preincubation of mutant ISG20 and RNA substrate decreases the RNase activity of wild-type ISG20 by up to 90 %, indicating that ISG20-D94G interacts with RNA more efficiently than wild type [15].

As mentioned above, ISG20 inhibited IAV polymerase activity, so we wondered whether ISG20 interacts with NP because NP encapsulates vRNA segments and associates

with the polymerase complex to form the viral ribonucleoprotein (vRNP) complex [33]. Our immunofluorescence and co-IP results revealed that ISG20 colocalizes and interacts with NP, but neither ISG20 nor ISG20-D94G affected the cellular localization of M1 and NP protein (Fig. 4a; data for M1 not shown). Moreover, neither ISG20 nor ISG20-D94G influenced the nuclear-cytoplasmic shuttling of NP protein. At the early stage of the IAV life cycle (4 h p.i.), the NP protein localized in the nucleus in both empty vector-transfected and ISG20(s)-expressing cells (data not shown). However, at the late stage of viral life cycle (12 h p.i.), the NP protein translocated into the cytoplasm in both the control and ISG20-expressing cells.

NP is a multi-functional protein of IAV, and several host factors were identified to interact with NP, and the interaction between NP and host factors exhibited its diverse role in viral life cycle [37–42]. The human anti-apoptosis protein clusterin (CLU) is targeted by NP to induced apoptosis [41]. Human heat-shock protein 40 (Hsp40) and cytoskeleton-scaffolding protein alpha-actinin-4 interact with NP to promote viral replication [38, 39]. Nevertheless, host protein Moloney leukemia virus 10 (MOV10) and tripartite motif protein superfamily member (TRIM22) interact with NP to inhibit viral replication [37, 42]. The interaction between MOV10 and NP results in the retention of NP in the cytoplasm, and the inhibitory effect is independent on its helicase activity. In contrast, ISG20 did not influence the cellular localization of NP, and the inhibitory effect was dependent on its exonuclease activity, indicating that ISG20 may define a novel antiviral pattern against IAV.

In conclusion, IAV induced the expression of ISG20, and ISG20 inhibited viral genome replication and transcription by interacting with the critical component of vRNP. These data indicated that ISG20 is a host factor that restricts the infection of IAV, and ISG20 may act as a promising antiviral drug candidate.

Acknowledgments This work was supported by grants from the Key Research Program of the Chinese Academy of Sciences (KSZD-EW-Z-005-001-1) and the National Natural Science Foundation of China (NSFC) (Grant Nos. 31402216, 81271849 and 31472178). WJL is the principal investigator of the NSFC Innovative Research Group (Grant No. 81321063).

Author contributions Designed and performed the experiments: HRQ, WJL, and HXH. Analyzed the data: HRQ, LMY, and LS. Wrote the paper: HRQ and JL, Modified the paper: WJL and HXH.

Compliance with ethical standards

Conflict of interest The authors declare that they have no conflict of interest.

Ethical approval This article does not contain any studies with human participants or animals performed by any of the authors.

References

1. B.W. Jagger, H.M. Wise, J.C. Kash, K.A. Walters, N.M. Wills, Y.L. Xiao, R.L. Dunfee, L.M. Schwartzman, A. Ozinsky, G.L. Bell, R.M. Dalton, A. Lo, S. Efstathiou, J.F. Atkins, A.E. Firth, J.K. Taubenberger, P. Digard, Science **337**, 199–204 (2012)
2. H.M. Wise, C. Barbezange, B.W. Jagger, R.M. Dalton, J.R. Gog, M.D. Curran, J.K. Taubenberger, E.C. Anderson, P. Digard, Nucleic Acids Res. **39**, 7775–7790 (2011)
3. H.M. Wise, A. Foeglein, J. Sun, R.M. Dalton, S. Patel, W. Howard, E.C. Anderson, W.S. Barclay, P. Digard, J. Virol. **83**, 8021–8031 (2009)
4. H.M. Wise, E.C. Hutchinson, B.W. Jagger, A.D. Stuart, Z.H. Kang, N. Robb, L.M. Schwartzman, J.C. Kash, E. Fodor, A.E. Firth, J.R. Gog, J.K. Taubenberger, P. Digard, PLoS Pathog. **8**, e1002998 (2012)
5. E.G. Brown, Biomed. Pharmacother. **54**, 196–209 (2000)
6. S. Tong, X. Zhu, Y. Li, M. Shi, J. Zhang, M. Bourgeois, H. Yang, X. Chen, S. Recuenco, J. Gomez, L.M. Chen, A. Johnson, Y. Tao, C. Dreyfus, W. Yu, R. McBride, P.J. Carney, A.T. Gilbert, J. Chang, Z. Guo, C.T. Davis, J.C. Paulson, J. Stevens, C.E. Rupprecht, E.C. Holmes, I.A. Wilson, R.O. Donis, PLoS Pathog. **9**, e1003657 (2013)
7. S. Tong, Y. Li, P. Rivailler, C. Conrardy, D.A. Castillo, L.M. Chen, S. Recuenco, J.A. Ellison, C.T. Davis, I.A. York, A.S. Turmelle, D. Moran, S. Rogers, M. Shi, Y. Tao, M.R. Weil, K. Tang, L.A. Rowe, S. Sammons, X. Xu, M. Frace, K.A. Lindblade, N.J. Cox, L.J. Anderson, C.E. Rupprecht, R.O. Donis, Proc. Natl. Acad. Sci. USA **109**, 4269–4274 (2012)
8. T. Watanabe, Y. Kawaoka, Curr Opin Virol. **14**, 71–78 (2015)
9. W. Zou, D. Chen, M. Xiong, J. Zhu, X. Lin, L. Wang, J. Zhang, L. Chen, H. Zhang, H. Chen, M. Chen, M. Jin, Sci Rep. **3**, 1601 (2013)
10. D.C. Munday, E. Emmott, R. Surtees, C.H. Lardeau, W. Wu, W.P. Duprex, B.K. Dove, J.N. Barr, J.A. Hiscox, Mol. cell. proteom. **9**, 2438–2459 (2010)
11. L. Liu, J. Zhou, Y. Wang, R.J. Mason, C.J. Funk, Y. Du, J. Proteom. Res. **11**, 4091–4101 (2012)
12. N. Lietzen, T. Ohman, J. Rintahaka, I. Julkunen, T. Aittokallio, S. Matikainen, T.A. Nyman, PLoS Pathog. **7**, e1001340 (2011)
13. K.M. Coombs, A. Berard, W. Xu, O. Krokhin, X. Meng, J.P. Cortens, D. Kobasa, J. Wilkins, E.G. Brown, J. Virol. **84**, 10888–10906 (2010)
14. C. Gongora, G. David, L. Pintard, C. Tissot, T.D. Hua, A. Dejean, N. Mechti, J. Biol. Chem. **272**, 19457–19463 (1997)
15. L.H. Nguyen, L. Espert, N. Mechti, D.M. Wilson 3rd, Biochemistry **40**, 7174–7179 (2001)
16. T. Horio, M. Murai, T. Inoue, T. Hamasaki, T. Tanaka, T. Ohgi, FEBS Lett. **577**, 111–116 (2004)
17. S.F. Wieland, R.G. Vega, R. Muller, C.F. Evans, B. Hilbush, L.G. Guidotti, J.G. Sutcliffe, P.G. Schultz, F.V. Chisari, J. Virol. **77**, 1227–1236 (2003)
18. S. Wieland, R. Thimme, R.H. Purcell, F.V. Chisari, Proc. Natl. Acad. Sci. USA **101**, 6669–6674 (2004)
19. C. Prehaud, F. Megret, M. Lafage, M. Lafon, J. Virol. **79**, 12893–12904 (2005)
20. J. Yuan, E. Cahir-McFarland, B. Zhao, E. Kieff, J. Virol. **80**, 2548–2565 (2006)
21. K.A. Simmen, J. Singh, B.G. Luukkonen, M. Lopper, A. Bittner, N.E. Miller, M.R. Jackson, T. Compton, K. Fruh, Proc. Natl. Acad. Sci. USA. **98**, 7140–7145 (2001)
22. M.A. Zahoor, G. Xue, H. Sato, Y. Aida, Virus Res. **208**, 156–163 (2015)

23. L. Espert, G. Degols, C. Gongora, D. Blondel, B.R. Williams, R.H. Silverman, N. Mechti, J. Biol. Chem. **278**, 16151–16158 (2003)
24. D. Jiang, H. Guo, C. Xu, J. Chang, B. Gu, L. Wang, T.M. Block, J.T. Guo, J. Virol. **82**, 1665–1678 (2008)
25. Z. Zhou, N. Wang, S.E. Woodson, Q. Dong, J. Wang, Y. Liang, R. Rijnbrand, L. Wei, J.E. Nichols, J.T. Guo, M.R. Holbrook, S.M. Lemon, K. Li, Virology **409**, 175–188 (2011)
26. L. Espert, G. Degols, Y.L. Lin, T. Vincent, M. Benkirane, N. Mechti, J. Gen. Virol. **86**, 2221–2229 (2005)
27. Y. Hao, D. Yang, J. Huazhong Univ. Sci. Technol. Med. Sci. **28**, 11–13 (2008)
28. T.P. Koestler, D. Rieman, K. Muirhead, R.G. Greig, G. Poste, Proc. Natl. Acad. Sci. USA **81**, 4505–4509 (1984)
29. Z. Wang, X. Liu, Z. Zhao, C. Xu, K. Zhang, C. Chen, L. Sun, G.F. Gao, X. Ye, W. Liu, PLoS One **6**, e22625 (2011)
30. L. Hou, J. Li, H. Qu, L. Yang, Y. Chen, Q. Du, W. Liu, Chin. J. Biotech. **31**, 123–134 (2015)
31. H. Qu, L. Yang, S. Meng, L. Xu, Y. Bi, X. Jia, J. Li, L. Sun, W. Liu, PLoS One **8**, e59307 (2013)
32. X. Jia, Y. Bi, J. Li, Q. Xie, H. Yang, W. Liu, Sci. rep. **5**, 10651 (2015)
33. W. Zheng, J. Li, S. Wang, S. Cao, J. Jiang, C. Chen, C. Ding, C. Qin, X. Ye, G.F. Gao, W. Liu, J. Virol. **89**, 5822–5834 (2015)
34. A. Pichlmair, C. Lassnig, C.A. Eberle, M.W. Gorna, C.L. Baumann, T.R. Burkard, T. Burckstummer, A. Stefanovic, S. Krieger, K.L. Bennett, T. Rulicke, F. Weber, J. Colinge, M. Muller, G. Superti-Furga, Nat. Immunol. **12**, 624–630 (2011)
35. J. Yu, D. Wang, J. Jin, J. Xu, M. Li, H. Wang, J. Dou, C. Zhou, Antivir. Res. **127**, 68–78 (2016)
36. Y. Sasaki, M. Kakisaka, N. Chutiwitoonchai, S. Tajima, H. Hikono, T. Saito, Y. Aida, Biochem. Biophys. Res. Commun. **450**, 49–54 (2014)
37. J. Zhang, F. Huang, L. Tan, C. Bai, B. Chen, J. Liu, J. Liang, C. Liu, S. Zhang, G. Lu, Y. Chen, H. Zhang, J. Virol. **90**, 3966–3980 (2016)
38. J. Batra, S. Tripathi, A. Kumar, J.M. Katz, N.J. Cox, R.B. Lal, S. Sambhara, S.K. Lal, Sci. Rep. **6**, 19063 (2016)
39. S. Sharma, A.K. Mayank, H. Nailwal, S. Tripathi, J.R. Patel, J.B. Bowzard, P. Gaur, R.O. Donis, J.M. Katz, N.J. Cox, R.B. Lal, H. Farooqi, S. Sambhara, S.K. Lal, FEBS J. **281**, 2899–2914 (2014)
40. A. Generous, M. Thorson, J. Barcus, J. Jacher, M. Busch, H. Sleister, Virol. J. **11**, 228 (2014)
41. S. Tripathi, J. Batra, W. Cao, K. Sharma, J.R. Patel, P. Ranjan, A. Kumar, J.M. Katz, N.J. Cox, R.B. Lal, S. Sambhara, S.K. Lal, Cell Death Dis. **4**, e562 (2013)
42. A. Di Pietro, A. Kajaste-Rudnitski, A. Oteiza, L. Nicora, G.J. Towers, N. Mechti, E. Vicenzi, J. Virol. **87**, 4523–4533 (2013)